A comparison of numerical solutions of the one-dimensional unsaturated–saturated flow and mass transport equations*

M. Th. VAN GENUCHTEN
US Salinity Laboratory, USDA, ARS, 4500 Glenwood Drive, Riverside, CA 92501, USA

INTRODUCTION

The simultaneous transport of water and solutes under transient unsaturated–saturated conditions plays an important role in many branches of agriculture and engineering. In agriculture, for example, many chemicals such as fertilizers, pesticides, as well as those naturally present in irrigation waters, are routinely applied to the field. Some of these chemicals will remain in the root zone or will be taken up by plant roots, while others are subject to leaching, thereby becoming potential groundwater pollutants. The frequent use of land for the disposal of a wide variety of domestic and industrial wastes further accentuates the importance of the unsaturated zone. A clear understanding of chemical transport in the unsaturated zone, including proper quantification of the relevant transport processes, is therefore important for both agricultural and environmental engineers. Extensive research in this area has led to a large number of papers dealing with unsaturated zone transport. Most of the earlier numerical studies have used finite difference techniques for solution of the governing equations[1–4], although recently also several finite element solutions have been published[5,6]. It is the purpose of this paper to compare the accuracy and computational efficiency of several numerical schemes for solution of the governing one-dimensional flow and mass transport equations.

GOVERNING EQUATIONS

One-dimensional vertical flow of water in an unsaturated–saturated medium is described by

$$L_w(h) \equiv \frac{\partial}{\partial x}\left(K\frac{\partial h}{\partial x} - K\right) - C\frac{\partial h}{\partial t} = 0 \qquad (1)$$

where C = the specific moisture capacity, h = the pressure head, K = the hydraulic conductivity, x = the vertical coordinate (positive down), t = the time. The coefficient C in equation (1) is given by:

$$C = \frac{\theta}{\varepsilon}S_s + \varepsilon\frac{\partial S_w}{\partial h} \qquad (2)$$

where θ = the volumetric moisture content, ε = the porosity, S_s = the specific storage coefficient, S_w = the degree of fluid saturation.

The second term on the right-hand side of equation (2) is zero for a fully saturated medium. The term containing S_s, on the other hand, can often be neglected when only an unsaturated zone is present. C in that case can be closely approximated by the slope of the soil moisture retention curve, $\theta(h)$:

$$C \simeq \frac{\partial \theta}{\partial h} \qquad (3)$$

The governing equation for chemical transport is taken as:

$$L_s(c) \equiv \frac{\partial}{\partial x}\left(\theta D\frac{\partial c}{\partial x} - qc\right) - \frac{\partial}{\partial t}(\theta c + \rho S) = 0 \qquad (4)$$

where c = the solution concentration, D = the dispersion coefficient, S = the adsorbed concentration, q = the volumetric flux, ρ = the bulk density.

The solution of equation (4) requires knowledge of both θ and q. θ is assumed to be a unique function of h, and can therefore be obtained from solutions of equation (1). Also q follows immediately from solutions of equation (1) by making use of Darcy's law as follows:

$$q = -K\frac{\partial h}{\partial x} + K \qquad (5)$$

The dispersion coefficient (D) represents the effects of both molecular diffusion and mechanical dispersion, and is assumed to be adequately defined by:

$$D = D_0\tau + \lambda|v| \qquad (6)$$

where D_0 = the molecular diffusion coefficient, τ = the tortuosity factor, λ = the dispersivity, v = the average pore-water velocity: $v = q/\theta$.

The solution of equation (4) requires also an expression relating the adsorbed concentration (S) with the solution concentration (c). This study considers only single-ion equilibrium transport, and the general adsorption isotherm is described by a linear (or linearized) isotherm of the form:

$$S = kc \qquad (7)$$

where k is an empirical distribution coefficient. Substitution of equation (7) into equation (4) gives the

* Presented at Third International Conference on Finite Elements in Water Resources, University of Mississippi, May 1980

0309-1708/82/010047-09$2.00

form of the mass transport equation used here:

$$L_s(c)\equiv\frac{\partial}{\partial x}\left(\theta D\frac{\partial c}{\partial x}-qc\right)-\frac{\partial}{\partial t}(\theta Rc)=0 \tag{8}$$

where the retardation factor R is defined as:

$$R=1+\frac{\rho k}{\theta} \tag{9}$$

NUMERICAL SOLUTION OF THE FLOW EQUATION

Equations (1) and (8) will be solved using the Galerkin-finite element method. Because this method has been discussed at length elsewhere[7,8], only the most pertinent steps in the solution procedure will be given here. Additional details are given by van Genuchten[9,10]. In the finite element approach the dependent variable, h, is approximated by a finite series of the form:

$$h(x,t)\simeq\hat{h}(x,t)=\sum_{j=1}^{n}\varphi_j(x)a_j(t) \tag{10}$$

where the $\varphi_j(x)$ are the selected basic functions and the $a_j(t)$ the associated, unknown, time-dependent coefficients which represent solutions of equation (1) at specified nodes within the solution domain. The Galerkin approach requires that the residual $L_w(\hat{h})$, obtained by substituting equation (10) into (1), be orthogonal to each of the n selected basis functions:

$$\int_0^l L_w\left[\sum_{j=1}^{n}\varphi_j(x)a_j(t)\right]\varphi_i(x)\mathrm{d}x=0 \quad i=1,2,\ldots,n \tag{11}$$

where l is the depth of the simulated soil profile ($0\leqslant x\leqslant l$). Substituting equation (1) into (11) and applying integration by parts to the spatial derivatives leads to the matrix equation:

$$[A]\{X\}+[B]\left\{\frac{\mathrm{d}X}{\mathrm{d}t}\right\}=\{F\} \tag{12}$$

where

$$[A_{ij}]=\int_0^l K\frac{\mathrm{d}\varphi_j}{\mathrm{d}x}\frac{\mathrm{d}\varphi_i}{\mathrm{d}x}\mathrm{d}x \tag{13a}$$

$$[B_{ij}]=\int_0^l C\varphi_j\varphi_i\mathrm{d}x \tag{13b}$$

$$\{X_i\}=\{a_i\} \tag{13c}$$

$$\{F_i\}=-\hat{q}\varphi_i\Big|_0^l+\int_0^l K\frac{\mathrm{d}\varphi_i}{\mathrm{d}x}\mathrm{d}x \tag{13d}$$

$$\hat{q}=-\left(K\frac{\partial\hat{h}}{\partial x}-K\right) \tag{13e}$$

Equation (12) defines a set of n ordinary differential equations with non-linear coefficients. A finite difference scheme may be introduced to approximate the time derivative in the matrix equation. Define for that purpose the following approximations:

$$\left\{\frac{\mathrm{d}X}{\mathrm{d}t}\right\}^{t+\Delta t/2}\simeq\frac{\{X\}^{t+\Delta t}-\{X\}^{t}}{\Delta t} \tag{14a}$$

$$\{X\}^{t+\Delta t/2}\simeq\omega\{X\}^{t+\Delta t}+(1-\omega)\{X\}^{t} \tag{14b}$$

where Δt is the time step and ω a temporal weighting coefficient. By defining matrix equation (12) at the half-time level $(t+\Delta t/2)$, and introducing approximations (14a) and (14b), the following set of n algebraic equations results:

$$[P]^{t+\Delta t/2}\{X\}^{t+\Delta t}=[Q]^{t+\Delta t/2}\{X\}^{t}+\{F\}^{t+\Delta t/2} \tag{15}$$

where

$$[P]=\omega[A]+\frac{1}{\Delta t}[B] \tag{16a}$$

$$[Q]=(\omega-1)[A]+\frac{1}{\Delta t}[B] \tag{16b}$$

When $\omega=1$ an implicit in time finite difference scheme results, even though the various coefficients are evaluated at the half-time level[6,11]. When $\omega=1/2$, on the other hand, a time-centred, Crank–Nicolson type algorithm is obtained[12].

To be able to solve equation (15), one needs estimates of the coefficients K and C in equation (13) at the half-time level. Because these coefficients depend on the pressure head, it is necessary to have an estimate of the pressure head distribution, h, at the half-time level. For each new time step this distribution is obtained through linear extrapolation from the old distributions as follows:

$$\hat{h}^{t+\Delta t/2}=\hat{h}^{t}+\frac{\Delta t_n}{2\Delta t_0}(\hat{h}^{t}-\hat{h}^{t-\Delta t}) \tag{17}$$

where Δt_0 and Δt_n are the old and new time increments, respectively. Because equation (5) is non-linear, the initial estimate must be improved by means of an iterative process. During each iteration the most recent distribution of $h^{t+\Delta t}$, obtained by solving equation (15) and making use of equation (10), is used to obtain a new estimate for the half-time level:

$$\hat{h}^{t+\Delta t/2}=\frac{1}{2}(\hat{h}^{t+\Delta t}+\hat{h}^{t}) \tag{18}$$

The iterative process continues until a satisfactory degree of convergence is obtained. The criterion of convergence, in its most general form, is given by:

$$|\hat{h}_i^{k+1}-\hat{h}_i^{k}|\leqslant\mu_1+\mu_2|\hat{h}_i^{k+1}| \tag{19}$$

where k represents the iteration number, $h_i=h(x_i)$, and where μ_1 and μ_2 are the selected absolute and relative error criteria.

Basis functions

Equation (15) will be solved for two sets of basis functions: zero-order continuous linear and first-order continuous cubic Hermitian basis functions. For each linear element, equation (10) reduces to:

$$\hat{h}(x,t)=\varphi_1^0(x)H_1(t)+\varphi_2^0(x)H_2(t) \tag{20}$$

where $H_1(t)$ and $H_2(t)$ represent the unknown pressure head values at the two corner nodes of the element. The basis functions can be written in terms of a local (ξ) coordinate system, as follows:

$$\varphi_j^0=\frac{1}{2}(1+\xi_0\xi) \qquad \xi_0=\pm 1 \tag{21}$$

where

$$\xi=\frac{2(x-x_1)}{\Delta x}-1 \qquad (x_1\leqslant x\leqslant x_2) \tag{22}$$

and where $\Delta x=(x_2-x_1)$ represents the nodal distance of the element.

In the case of the Hermitian basis functions, one not only solves for the function itself, but also for its spatial derivatives. Equation (10), as applied to each local element, reduces to:

$$\hat{h}(x,t)=\sum_{j=1}^{2}\left[\varphi_{0j}^1(x)H_j(t)+\varphi_{1j}^1(x)\frac{\mathrm{d}H_j}{\mathrm{d}x}(t)\right] \tag{23}$$

where

$$\varphi_{0j}^1=-\frac{1}{4}(\xi+\xi_0)^2(\xi\xi_0-2) \qquad (\xi_0=\pm 1) \tag{24a}$$

$$\varphi_{1j}^1=\frac{\Delta x}{8}\xi_0(\xi+\xi_0)^2(\xi\xi_0-1) \qquad (\xi_0=\pm 1) \tag{24b}$$

Numerical implementation

At least two approaches are possible to evaluate the integrals in the coefficient matrices (13). One possible approach is to expand the non-linear coefficients K and C in terms of the basis functions and the values of K and C at the nodes, analogous to equations (20) and (23). This approach was used for the linear finite element scheme, the advantage being that the relatively simple integrations in equation (13) need to be carried out only once. When applied to the coefficient C in equation (13b), for example, we have:

$$C(\xi)=C_1\varphi_1^0(\xi)+C_2\varphi_2^0(\xi) \tag{25}$$

where C_1 and C_2 represent the nodal values of C. Substituting equation (25) into equation (13b), using equations (21) and (22) for the integrations, and assuming an equal spacing between the nodes (constant Δx) leads then to the following approximation of $[B]$ (only the tridiagonal entries of the ith row of the matrix are given):

$$[B_{ij}]=\frac{\Delta x}{12}[C_{i-1}+C_i \quad C_{i-1}+6C_i+C_{i+1} \quad C_i+C_{i+1}] \tag{26}$$

For the more general case of variable Δx, the above matrix will become somewhat more complicated; the derivation, however, remains essentially the same.

Another possible approach for evaluating the integrals in equation (13) would be through the use of a numerical integration method, for example by using Gaussian quadrature. A disadvantage of this approach is that the integrations now have to be carried out during each iteration within each time step. The first approach was taken in conjunction with linear finite elements, since this approach resulted in a computationally more efficient scheme, while the accuracy remained approximately the same. Poor results, however, were obtained when the first approach was used for the Hermitian basis functions. The method, which requires evaluation of ($\mathrm{d}K/\mathrm{d}x$) and ($\mathrm{d}C/\mathrm{d}x$) at the nodes, produced severe oscillations in computed pressure head distributions and also introduced serious mass balance errors when infiltration in relatively dry soil was simulated. The second approach, numerical integration, was hence used for the Hermitian scheme. Several methods are available for this integration, such as Gaussian and Lobatto integration (see equations 25.4.29 and 25.4.32 of Abramowitz and Stegun[13], respectively). While a Gaussian integration scheme is probably the most accurate for a given number of integration points, it does not take full advantage of the properties of the Hermitian basis functions. Inspection of these functions (equation 24) shows that they become zero at one (φ_{0j}^1) or both corner nodes (φ_{1j}^1). The computational effort hence can be reduced by locating some of the integration points at the nodes ('Lobatto' integration).

An alternative finite element formulation may be developed based on the lumped-mass approach. Such an approach was first used by Neuman[12] to speed up numerical convergence when simulating infiltration into extremely dry soil. Mass-lumping is achieved by defining the nodal values of the time derivative as weighted averages over the entire flow region as:

$$\int_0^l C\frac{\partial h}{\partial t}\varphi_i\mathrm{d}x=\frac{\partial H_i}{\partial t}\int_0^l C\varphi_i\mathrm{d}x \tag{27}$$

Application of equation (27) will lead to a different coefficient matrix for the time derivative (matrix B, equation 13b). For example, for linear finite elements one obtains:

$$[B_{ij}]=\frac{\Delta x}{6}[0 \quad C_{i-1}+4C_i+C_{i+1} \quad 0] \tag{28}$$

The diagonal entries in equation (28) are identical to the row sums of the entries in equation (26). The mass-lumped linear finite element scheme can be further simplified by redefining $[B]$ as:

$$[B_{ij}]=\Delta x[0 \quad C_i \quad 0] \tag{29}$$

In this way a finite difference scheme is obtained. The complete finite difference expansion of equation (15) is:

$$a\,h_{i-1}^{t+\Delta t}+b\,h_i^{t+\Delta t}+d\,h_{i+1}^{t+\Delta t}=f \tag{30}$$

where

$$a=\frac{-\omega}{2\Delta x}(K_{i-1}+K_i) \tag{31a}$$

$$b=\frac{\Delta x}{\Delta t}C_i+\frac{\omega}{2\Delta x}(K_{i-1}+2K_i+K_{i+1}) \tag{31b}$$

$$d=\frac{-\omega}{2\Delta x}(K_i+K_{i+1}) \tag{31c}$$

$$f=-h_{i-1}^t\left[\frac{(\omega-1)}{2\Delta x}(K_{i-1}+K_i)\right]-h_{i+1}^t\left[\frac{(\omega-1)}{2\Delta x}(K_i+K_{i+1})\right]+$$

$$h_i^t\left[\frac{\Delta x}{\Delta t}C_i+\frac{(\omega-1)}{2\Delta x}(K_{i-1}+2K_i+K_{i+1})\right]+\frac{1}{2}(K_{i-1}-K_{i+2}) \tag{31d}$$

NUMERICAL SOLUTION OF THE TRANSPORT EQUATION

Application of the finite element method to the solution of the transport equation leads to an equation similar to (12). This equation shows that the finite element method is used only to approximate the spatial derivatives, while the time derivative has been left intact. The common approach, as used earlier for the flow equation, is to apply finite difference techniques to the resulting matrix equation (equation 12). This approach leads to a numerical scheme which is at most second-order correct in time (i.e., when $\omega=0.5$ in equation 15). Earlier studies[14,15] have shown that this procedure frequently leads to oscillatory solutions when a sharp concentration front is present. By using an implicit scheme, which is first-order correct in time, one can avoid most of the oscillations, but this will usually be at the expense of a smeared (too dispersed) concentration front. Some of the problems associated with the presence of oscillations and excessive numerical dispersion can be eliminated by making use of a higher-order integration scheme for the time-derivative in the transport equation. Such a higher-order scheme will become especially attractive when, as in this study, higher-order basis functions are used. It was shown earlier[15,16] that a third-order accurate temporal integration scheme can be obtained by introducing appropriate dispersion corrections into the numerical solution of the convective–dispersive equation at steady-state flow. Similar dispersion corrections can be derived for the transient problem[10]. For the present case this is accomplished by redefining equation (8) as:

$$L_s(c)\equiv\frac{(\theta Rc)^{t+\Delta t}-(\theta Rc)^t}{\Delta t}-$$

$$\frac{1}{2}\left[\frac{\partial}{\partial x}\left(\theta D^-\frac{\partial c}{\partial x}-qc\right)\right]^{t+\Delta t}-\frac{1}{2}\left[\frac{\partial}{\partial x}\left(\theta D^+\frac{\partial c}{\partial x}-qc\right)\right]^t=0 \tag{32}$$

where

$$D^-=D-\frac{q^2\Delta t}{6\theta^2R};\quad D^+=D+\frac{q^2\Delta t}{6\theta^2R} \tag{33}$$

Equation (32) is a time-centred, Crank–Nicolson type scheme with correction factors applied to the dispersion coefficient.

The finite element analysis, starting with equation (32) instead of equation (8), proceeds along the same line as for the flow equation. Substitution of L_s (equation 32) for L_w in equation (11) and integration by parts of the spatial derivatives yields:

$$[P]^{t+\Delta t}\{X\}^{t+\Delta t}=[Q]^t\{X\}^t+\{S\} \tag{34}$$

where

$$[P_{ij}]=\int_0^l\left[\frac{1}{2}\left(\theta D^-\frac{d\varphi_j}{dx}-q\varphi_j\right)\frac{d\varphi_i}{dx}+\frac{\theta R}{\Delta t}\varphi_j\varphi_i\right]dx \tag{35a}$$

$$[Q_{ij}]=\int_0^l\left[-\frac{1}{2}\left(\theta D^+\frac{d\varphi_j}{dx}-q\varphi_j\right)\frac{d\varphi_i}{dx}+\frac{\theta R}{\Delta t}\varphi_j\varphi_i\right]dx \tag{35b}$$

$$\{S_i\}=-\frac{1}{2}(q_s^{t+\Delta t}+q_s^t)\varphi_i\Big|_0^l \tag{35c}$$

$$q_s=-\theta D\frac{\partial\hat{c}}{\partial x}+q\hat{c} \tag{36}$$

EXAMPLE

An example will be used to compare the accuracy and computational efficiency of the four numerical schemes discussed in the previous sections, i.e., finite differences (FD), linear finite elements (LFE), mass-lumped linear finite elements (LFE), and Hermitian cubic finite elements (HFE). The example refers to a field infiltration experiment[17], in which water and chloride were allowed to infiltrate into a deep, homogeneous soil profile. The same experiment has been analysed numerically also by Bresler[2], Ungs *et al.*[18], Segol[6], and by Gureghian *et al.*[19]. The hydraulic properties of the soil are:

$$\theta(h)=\begin{cases}0.6829-0.09524\ \ln(|h|) & h\leqslant -29.484\\ 0.4531-0.02732\ \ln(|h|) & -29.484<h\leqslant -14.495\end{cases} \tag{37a}$$

$$K(h)=\begin{cases}19.34\times10^4\ |h|^{-3.4095} & h\leqslant -29.484\\ 516.8\ |h|^{-0.97814} & -29.484<h\leqslant -14.495\end{cases} \tag{37b}$$

where K is given in cm/day and h in cm. The initial and boundary conditions are:

$$\theta(x,0)=\begin{cases}0.1500+x/1200 & 0<x\leqslant 60\\ 0.2000 & 60<x\leqslant 125\end{cases} \tag{38a}$$

$$c(x,0)=0 \tag{38b}$$

$$h(0,t)=-14.495\qquad(\theta_0=0.38) \tag{38c}$$

$$c(0,t)=\begin{cases}209 & t<0.11667\\ 0 & t\geqslant 0.11667\end{cases} \tag{38d}$$

Table 1. Summary of numerical experiments for solution of the flow equation ($\mu_2=0$, $l=125$ cm, $\Delta t=$ variable)

Method*	Δx (cm)	Number of elements	μ_1 (cm)	Number of time steps	CPU time (sec)
FD	0.50	250	0.50	459	41.70
FD	1.00	125	0.50	326	15.32
FD	2.50	50	0.50	176	3.73
FD	5.00	25	0.50	108	1.44
FD	2.50	50	0.10	279	6.22
FD	2.50	50	0.25	212	4.54
FD	2.50	50	0.50	176	3.73
FD	2.50	50	1.00	146	3.27
FD	2.50	50	2.50	116	2.64
FD	2.50	50	0.50	176	3.73
LFE	2.50	50	0.50	170	3.86
MFE	2.50	50	0.50	174	3.82
5LP	5.00	25	0.50	156	9.41
2GP	5.00	25	0.50	132	6.60
3GP	5.00	25	0.50	170	9.91
4GP	5.00	25	0.50	149	10.19
4LP	5.00	25	0.50	145	7.92
5LP	5.00	25	0.50	156	9.41
5LP	5.00	25	0.50	156	9.41
5LP	5.00	25	1.00	133	8.52
5LP	5.00	25	2.50	105	6.89
5LP	5.00	25	0.50	156	9.41
5LP	7.50	17	0.50	118	4.98
5LP	10.00	13	0.50	94	3.30

* FD = finite differences
LFE = linear finite elements
MFE = mass-lumped linear finite elements
2GP = Hermitian finite elements (two Gauss points)
3GP = Hermitian finite elements (three Gauss points)
4GP = Hermitian finite elements (four Gauss points)
4LP = Hermitian finite elements (four Lobatto points)
5LP = Hermitian finite elements (five Lobatto points)

$$\frac{\partial h}{\partial x}(l,t)=0 \tag{38e}$$

$$\frac{\partial c}{\partial x}(l,t)=0 \tag{38f}$$

where x is given in cm, θ in cm^3/cm^3 and c in mequiv./l. Additional parameters are: $D_0\tau=0.6$ cm^2/day, $\lambda=1.026$ cm, $k=0$, and $l=125$ cm.

Table 1 gives a summary of the various computer runs, including the execution (CPU) times needed to complete the 0.4 day simultation on an IBM 360/91 computer. The execution times refer to solutions of the flow equation only; execution times for the combined flow and transport equations were approximately 100% higher. Computed moisture distributions are given in Figs. 1–5. The solid line in each Figure represents the assumed 'correct' solution, and was obtained by using increasingly smaller spatial and time increments until all four numerical schemes (FD, LFE, MFE, and HFE) generated essentially the same results. The correct solution was also found to be nearly identical to the three-term quasi-analytical solution of Philip[20] for relatively small times (Philip's solution diverges for large times).

The effects of different integration methods (equation 13) on results obtained with the Hermitian finite element scheme are shown in Fig. 1. The 2-point Gaussian (2GP) and 3-point Lobatto (3LP) integration schemes generate moisture distributions that not only lag considerably behind the correct solution, but also show some oscillatory behaviour, especially during the initial stages

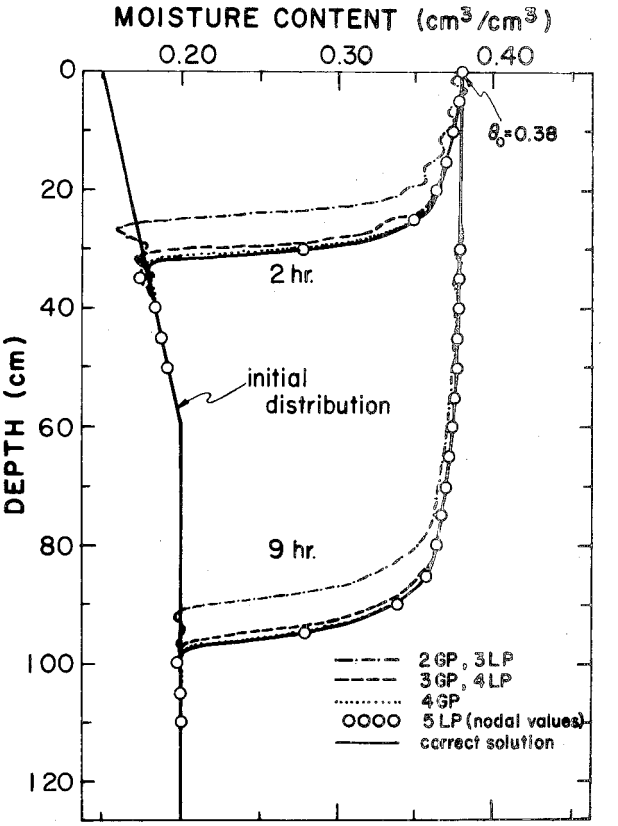

Figure 1. Effect of different numerical integration schemes on computed moisture profiles (Hermitian finite elements)

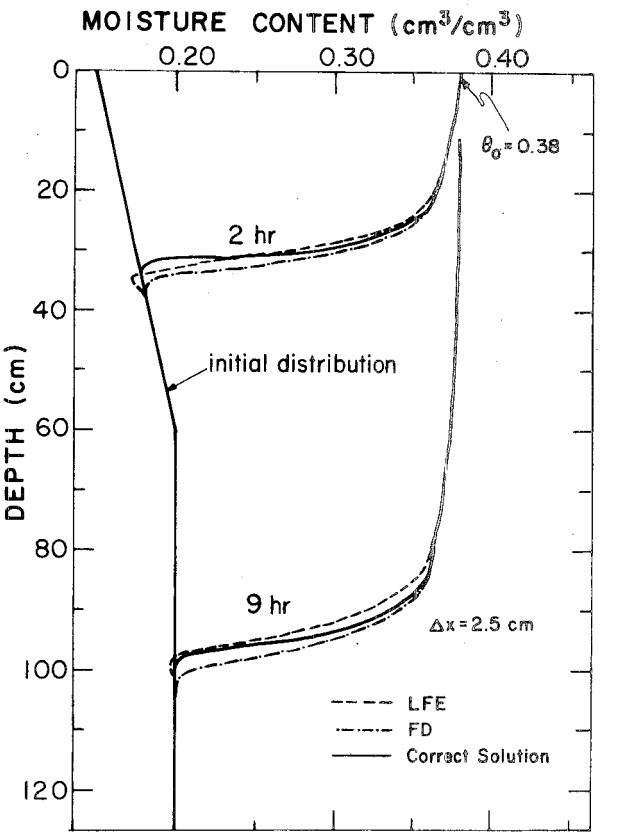

Figure 2. Moisture profiles obtained with finite differences (FD) and linear finite elements (LFE)

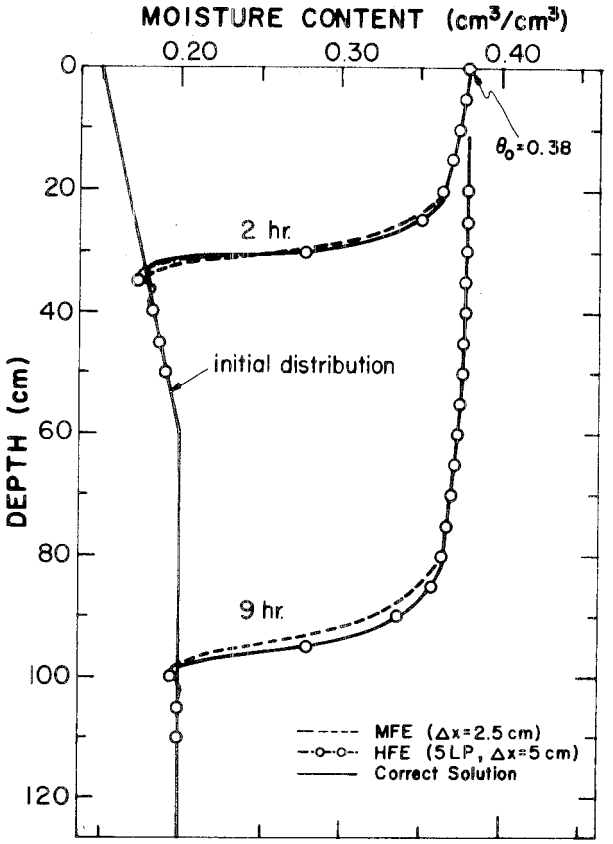

Figure 3. Moisture profiles obtained with mass-lumped (MFE) and Hermitian finite elements (HFE)

of infiltration. Much better results are obtained with the 3-point Gaussian (3GP) and 4-point Lobatto (4LP) integration schemes. These schemes, however, generate distributions which also lag behind the correct solution. The most accurate results were obtained with the 4-point Gaussian (4GP) and 5-point Lobatto (5LP) schemes. Actually, the 5LP-scheme is slightly better than the 4GP-scheme, even though the execution time is less than for the 3GP-scheme (Table 1).

Results obtained with finite differences (FD) and linear finite elements (LFE) are presented in Fig. 2, while Fig. 3 shows results obtained with mass-lumped linear finite elements (MFE) and Hermitian finite elements (HFE, 5LP). A constant spatial increment (Δx) of 2.5 cm was used for the three zero-order continuous schemes (FD, LFE, and MFE), while the HFE-scheme used a Δx of 5 cm (see also Table 1). Note that the FD- and LFE-schemes generate solutions which deviate slightly from the correct one, and that the computed moisture fronts are somewhat smeared in comparison with the HFE-scheme. Results obtained with the MFE-scheme (Fig. 3) are nearly identical to those obtained with the LFE-scheme (Fig. 2), except near the toe of the computed moisture fronts. No oscillations were observed when mass-lumping was applied to the linear finite element scheme.

While Figs. 2 and 3 demonstrate that the C^1 continuous Hermitian finite element scheme generates the most accurate results, Table 1 also shows that this scheme consumes approximately 2.5 times as much computer time as the various C^0 continuous schemes. The HFE-scheme hence does not immediately present an attractive alternative to the other schemes, unless its relative accuracy does not change dramatically with increasing element size. The effects of changing Δx on computed moisture distributions for FD and HFE are shown in Figs. 4 and 5, respectively. Doubling the spatial increments causes the computed front to move further ahead of the correct solution in the case of FD, while the front itself also becomes more dispersed. The execution time, on the other hand, decreases from 3.7 to 1.4 sec (Table 1). A doubling of the element size in the HFE-scheme still leads to a fairly accurate description of the moisture front (Fig. 5), although now some more serious oscillations appear. The computer time in this case is reduced from 9.4 to 3.3 sec.

Computed chloride distributions *versus* depth are shown in Figs. 6 and 7. The most accurate results are again obtained with the HFE-scheme. Also the FD- and MFE- schemes generate fairly accurate results, albeit less than for the HFE-scheme. Results obtained with the LFE-scheme are considerably less accurate than those for the other schemes. It appears that most of the observed deviations between the LFE results and the correct solution are generated during the early stages of infiltration (Fig. 6). Some serious oscillations in computed solute distributions are observed at that time, resulting in a deeper penetration of the solute front after two hours.

Figures 1–7 demonstrate that the Hermitian finite element scheme generates solutions which are superior to those obtained with the three zero-order continuous

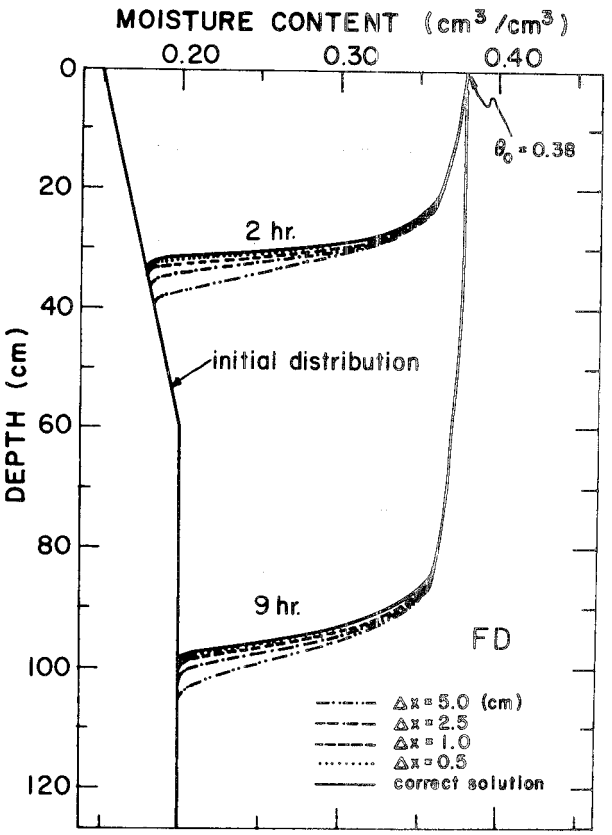

Figure 4. Effect of nodal spacing on computed moisture profiles using finite differences

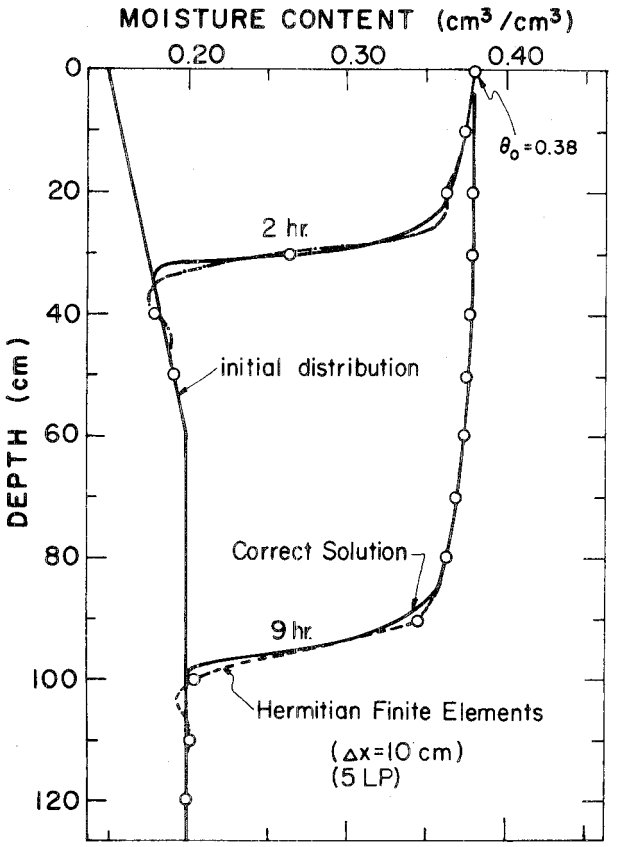

Figure 5. Comparison of Hermitian finite element solution (Δx = 10 cm) with correct solution

schemes. Unfortunately, this is accomplished with approximately twice as much computer time. Several reasons account for this. First, the HFE-scheme generates matrix equations for both flow and transport which have a bandwidth of 7, while the three C^0 continuous schemes produce matrix equations which have a bandwidth of only 3. Hence, more time is needed for solution of the Hermitian global matrix equation. Second, numerical integration techniques were used to evaluate the integrals of equation (13) for the HFE-scheme. This in itself already leads to more computer time but, in addition, forces one to a more time-consuming element by element assembly of the global matrix equations.

An accurate comparison of the efficiency of the different schemes is not easy because of the many parameters affecting the final results. All results thus far were obtained with a Crank–Nicolson scheme in time ($\omega = 0.5$ in equations 14 and 16). Execution times could be decreased by approximately 30% with an implicit scheme ($\omega = 1.0$). Computed moisture distributions in that case, however, generally lagged the correct solution, especially for the C^0 continuous schemes. Important reductions in execution time were also possible by increasing the integration tolerance parameters (μ_1 and μ_2 in 19). In the above example, μ_1 and μ_2 were set to 0.5 and 0.0, respectively. Approximately the same results were obtained when μ_1 was varied between 0.1 and 2.5 cm, although in some cases (notably for LFE and HFE) a few minor oscillations were observed in the calculated curves when μ_1 equalled 2.5 cm.

All curves thus far were obtained for a first-type, constant pressure boundary condition at the soil surface

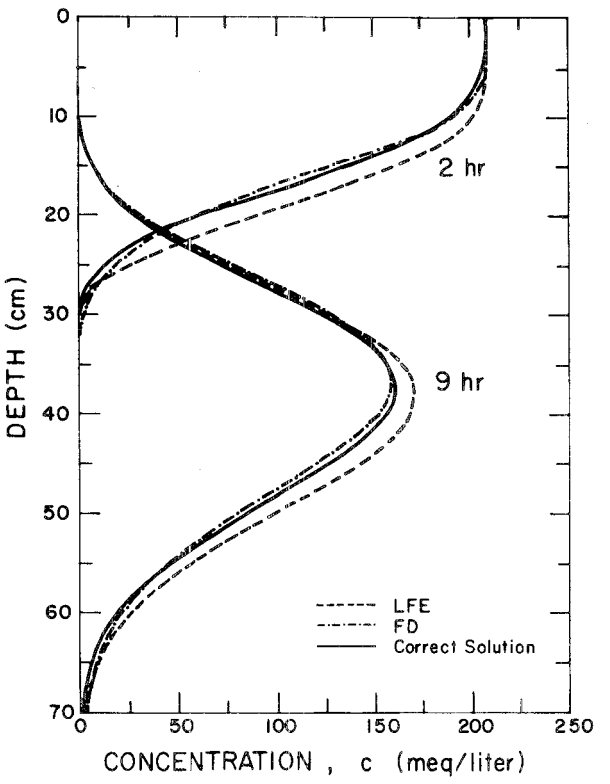

Figure 6. Chloride distributions obtained with finite differences (FD) and linear finite elements (LFE)

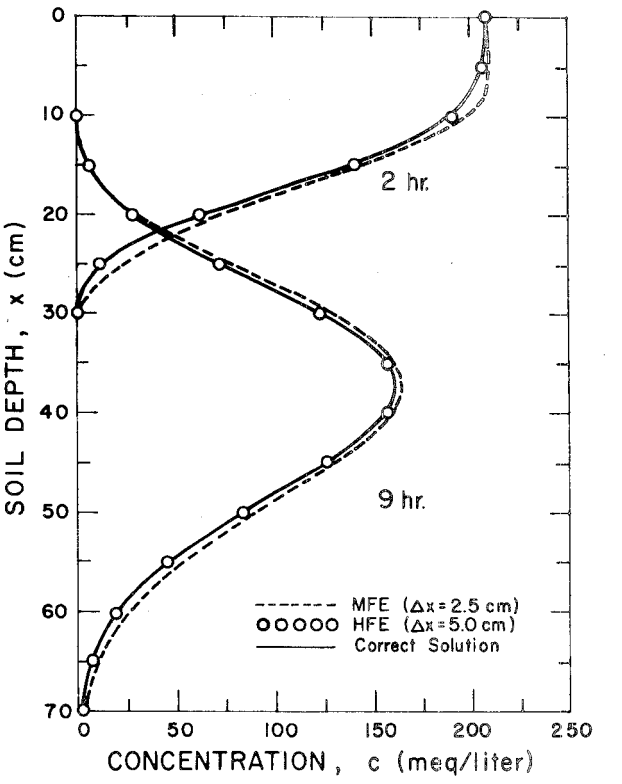

Figure 7. Chloride distributions obtained with mass-lumped linear (MFE) and Hermitian finite elements (HFE)

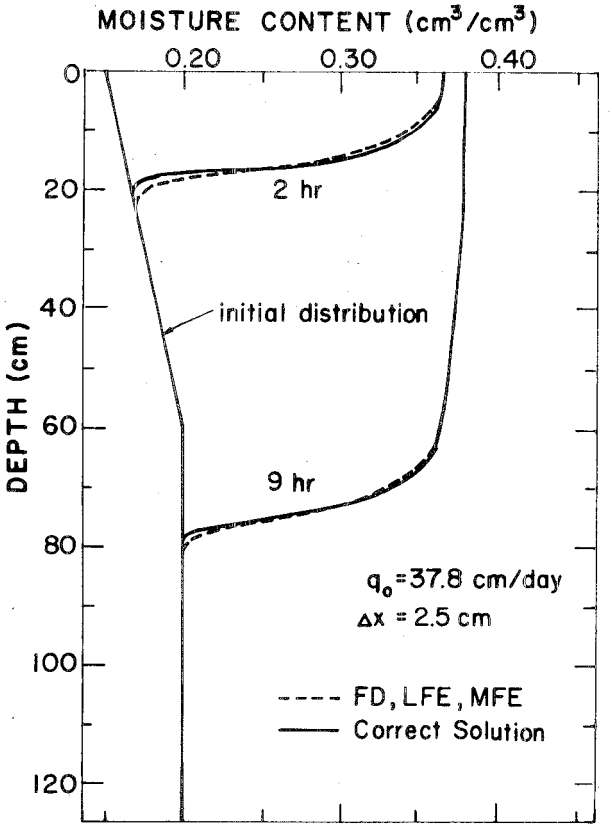

Figure 8. Comparison of finite difference (FD), linear finite element (LFE) and mass-lumped finite element (MFE) solutions with correct solution

(equation 38c). Several computer runs were also made for the case where a constant flux is given, i.e., for

$$\left(-K\frac{\partial h}{\partial x}+K\right)\Big|_{x=0}=q_0 \qquad (38)$$

where q_0 is the prescribed flux, assumed to be 37.8 cm/day (i.e., equal to the hydraulic conductivity at a moisture content of 0.38 cm^3/cm^3). Results for FD, LFE, and MFE are presented in Fig. 8. Note that the three schemes generate accurate solutions, although the computed fronts still remain slightly dispersed as compared to the correct front. The HFE-scheme was found to nearly duplicate the correct solution.

DISCUSSION

From the examples given here, and several other numerical experiments, it is concluded that the FD- and MFE-schemes will generate the most stable solutions when a steep moisture front is present (e.g., infiltration into a dry, coarse soil). These solutions, however, may diverge somewhat from the correct solutions when the simulation progresses in time, while the calculated moisture front could become more dispersed (smeared out) as compared to the correct front. The HFE-scheme (notably the 5LP-scheme) seems superior in locating the correct spatial location of the moisture front, while the calculated slope of the front is better described than with the various zero-order continuous schemes. However, some oscillations may develop near the toe of the front, especially when relatively large elements are present. Such oscillations are characteristic of those cases where a sharp moisture (or concentration) front needs to be simulated. It appears that, at least from a practical point of view, these oscillations are often of minor importance, especially if one is aware of their presence. For the experiments discussed here, for example, small oscillations in computed moisture distributions did not affect the accuracy of the calculated concentration profiles. The magnitude of the oscillations, furthermore, can often be decreased by using smaller spatial and time increments; this, of course, at the expense of more computer time. The more non-linear the flow problem, the more oscillations one may expect.

Several factors, other than those already discussed, will affect the accuracy and computational efficiency of a numerical scheme. For example, the programming details of the iterative scheme in the flow equation will greatly affect the efficiency of the program. These effects can easily be greater than the inherent differences between two numerical methods (e.g., between FD and HFE). The magnitude of the time step is also an important factor. A judicious choice of this parameter, including an automatic adjustment of Δt during execution, can greatly improve the efficiency of a program. The presence of adsorption and decay reactions, furthermore, will also influence the performance of a given numerical scheme. Larger spatial and time increments are often possible in the numerical solution of the transport equation when adsorption or decay processes are present. Unfortunately, adsorption and decay do not affect the solution scheme for the flow equation.

Another important consideration for selecting a certain numerical scheme is the required accuracy of the simulation results. The governing flow and transport equations contain several parameters which are difficult to measure in the field, and often have a large degree of uncertainty. Even the physical and chemical processes of unsaturated–saturated transport are sometimes poorly described by the governing equations. This suggests that the choice of a numerical scheme should be weighted against its potential use.

REFERENCES

1 Bresler, E. and Hanks, R. J. Numerical method for estimating simultaneous flow of water and salt in unsaturated soils, *Soil Sci. Soc. Am. Proc.* 1969, **33**, 827

2 Bresler, E. Simultaneous transport of solutes and water under transient unsaturated flow conditions, *Water Resourc. Res.* 1973, **9**, 975

3 Kirda, C., Nielsen, D. R. and Biggar, J. W. Simultaneous transport of chloride and water during infiltration, *Soil Sci. Soc. Am. Proc.* 1973, **37**, 339

4 Wood, A. L. and Davidson, J. M. Fluometuron and water content distributions during infiltration: measured and calculated, *Soil Sci. Soc. Am. Proc.* 1975, **39**, 820

5 Duguid, J. O. and Reeves, M. Material transport through porous media: a finite-element Galerkin model, *Oak Ridge National Laboratory, ORNL-4928*, 1976

6 Segol, G. A three-dimensional Galerkin-finite element model for the analysis of contaminant transport in saturated -unsaturated porous media, in *Finite Elements in Water Resources*, W. G. Gray *et al.* (Eds.), pp. 123–144, Pentech Press, London, 1977

7 Brebbia, C. A. and Connor, J. J. *Fundamentals of Finite Element Techniques for Structural Engineers*, Butterworths, London, 1974

8 Pinder, G. F. and Gray, W. G. *Finite Element Simulation in Surface and Subsurface Hydrology*, Academic Press, New York, 1977

9 van Genuchten, M. Th. Numerical solutions of the one-dimensional saturated-unsaturated flow equation, *Research Report 78-WR-9* 1978, Water Resources Program, Department of Civil Engineering, Princeton University

10 van Genuchten, M. Th. Mass transport in saturated-unsaturated media: one-dimensional solutions, *Research Report 78-WR-11*, 1978, Water Resources Program, Department of Civil Engineering, Princeton University

11 Frind, E. O., Gilham, R. W. and Pickens, J. F. Application of unsaturated flow properties in the design of geologic environments for radioactive waste storage facilities, in *Finite Elements in Water Resources*, (Eds. W. G. Gray *et al.*), pp. 133–163, Pentech Press, London

12 Neuman, S. P. Finite element computer programs for flow in saturated-unsaturated porous media, *Second A. Rep., No. A10-SWC-77*, Hydraul. Eng. Lab., Technion, Haifa, Israel, 1972

13 Abramowitz, M. and Stegun, I. A. *Handbook of Mathematical Functions*, Dover, New York, 1970

14 Gray, W. G. and Pinder, G. F. An analysis of the numerical solution of the transport equation, *Water Resour. Res.* 1976, **12**, 547

15 van Genuchten, M. Th. On the accuracy and efficiency of several numerical schemes for solving the convective-dispersive equation, in *Finite Elements in Water Resources*, (Eds. W. G. Gray *et al.*), pp. 71–90, Pentech Press, London, 1977

16 van Genuchten, M. Th. and Gray, W. G. Analysis of some dispersion corrected numerical schemes for solution of the transport equation, *Int. J. Num. Meth. Eng.* 1978, **12**, 387

17 Warrick, A. W., Biggar, J. W. and Nielsen, D. R. Simultaneous solute and water transfer for an unsaturated soil, *Water Resour. Res.* 1971, **7**, 1216

18 Ungs, M., Cleary, R. W., Boersma, L. and Yingjajaval, S. The quantitative description of transfer of water and chemicals through soils, in *Land as a Waste Management Alternative*, R. C. Loehr (Ed.), pp. 109–137, Ann Arbor Science, Ann Arbor, 1976

19 Gureghian, A. B., Ward, D. S. and Cleary, R. W. Simultaneous transport of water and reacting solutes through multilayered soils under transient unsaturated flow conditions, *J. Hydrol.* 1979, **41**, 253

20 Philip, J. R. Numerical solution of equations of the diffusion type with diffusivity concentration dependent. II, *Austr. J. Phys.* 1957, **10**, 29